Late Quaternary lateral sedimentation in the São Tomé Seamount area of the western South Atlantic

Dmitrii G. Borisov[1], Ivar O. Murdmaa[1], Elena V. Ivanova[1], and Evgenia V. Dorokhova[1]

Received 20 August 2019; accepted 5 November 2019; published 28 December 2019.

This work is focused on a problem of distinguishing between contourites and turbidites in the southwestern Brazil Basin, which is crucial for better understanding of the Late Quaternary history of interplay between along slope and down slope sedimentation processes in the western South Atlantic. The study embraces an area between the Almirante Saldanha and São Tomé Seamounts, which is not linked to any known depositional system. This area was not previously studied in frame of the contourite paradigm. Very high-resolution seismic records and lithological data acquired during three cruises of the RV *Akademik Ioffe* (2011–2013) revealed domination of lateral sedimentation in the area of the São Tomé Seamount. Interplay between along slope and gravity driven sedimentation processes interacting with the ocean floor topography resulted in the formation of complicated sediment structures and a wide range of seismic facies. Along slope sedimentation processes are controlled by the Antarctic bottom water current, which reworked coarse-grained material derived from the continental slope through turbidity flows. The study area is divided into two zones, which are characterized by domination of either gravity flows or bottom current related sedimentation processes. The São Tomé Seamount marks a boundary between these zones. The obtained results improved knowledges about the formation history of the Upper Quaternary sediment cover on the continental rise of the southwestern Brazil Basin and about interplay between gravity-driven and bottom current related sedimentation processes during the last glacial-interglacial cycle. *KEYWORDS:* Contourites; turbidites; continental rise; bottom current; AABW; seismic profiling; seismic facies.

Citation: Borisov, Dmitrii G., Ivar O. Murdmaa, Elena V. Ivanova, and Evgenia V. Dorokhova (2019), Late Quaternary lateral sedimentation in the São Tomé Seamount area of the western South Atlantic, *Russ. J. Earth. Sci., 19,* ES6014, doi:10.2205/2019ES000689.

1. Introduction

Interplay between downslope and along slope sedimentation processes played a crucial role in sediment cover formation along the South American oceanic margin during the Quaternary. First, this sediment cover concerns an interaction between turbidity flows and geostrophic (contour) currents, as their simultaneous action or alternation through time in response to global climate changes, sea-level variations and tectonic movements remains questionable. This is mainly due to a lack of unambiguous criteria for distinguishing between contourites and fine-grained distal turbidites. The southern part of the Brazil Basin is characterized by a number of mixed contourite-turbidite systems, which

[1]Shirshov Institute of Oceanology RAS, Moscow, Russia

http://rjes.wdcb.ru/doi/2019ES000689-res.html

represents a perfect area for investigation of both types of lateral sedimentation processes. However, the sediment sections and paleoceanographic records on the continental rise and in the contiguous abyssal part of the basin remain poorly studied. Previous studies which were also focused on the lateral sedimentation during the Quaternary embraced two depositional systems east and west of the study area [*Faugères et al.,* 2002; *Gonthier et al.,* 2003; *Lima et al.,* 2009]. These papers demonstrated the complexity and variety of interactions between gravity driven and bottom current related processes. The low carbonate content in sediments, frequent hiatuses and sediment reworking allowed neither establishing of reliable stratigraphy for cores nor the detailed investigation of lateral sedimentation in relation to global climate changes during the Late Quaternary. The available maps of echo facies distribution in the south-western Brazil Basin have insufficient resolution for detailed study of sedimentation processes in the area of the São Tomé seamount [e.g. *Damuth and Hayes,* 1977], so one of the main focuses of this paper is the detailed investigation of echo character types on the base of very high resolution seismic records. The main aim of this work is to cover (partly) the gap between the Columbia Channel depositional system and the São Tomé deep-sea channel levee system and to study the interplay between gravity driven and bottom current related processes, which occurred in this area during the last glacial-interglacial cycle.

1.1. Seafloor Topography and Geological Setting

In the southwestern Brazil Basin, the continental rise is confined by the Rio Grande Rise in the south and the Vitoria-Trindade Seamounts in the north. The escarpment of the São Paulo Plateau in the west is characterized by a smooth surface, which gently slopes eastward. In addition to the W–E extending Vitoria-Trindade chain, there are two, conically shaped seamounts: the Almirante Saldanha and São Tomé (Figure 1A, Figure 1B). The São Tomé Seamount is approximately 37 km × 42 km with a relative height of 2800 m (minimum water depth of 1350 m). The height of the Almirante Saldanha Seamount exceeds 3600 m and its dimensions are approximately 47 × 58 km.

The large São Paulo Plateau is located on the continental slope at a depth range of 2000–3200 m. The eastern boundary of the plateau is marked by a 200-m-high escarpment with a N–S trend. The plateau is affected by numerous halokinetic structures related to the Aptian salt deposits. The active diapiric structures control the courses of the manifold channels that form a complex network on the plateau [*Viana et al.,* 2003]. Some of these channels cross the escarpment extend to the rise, which converge and form several major channels [*Gonthier et al.,* 2003]. The most prominent channel in the area is the Columbia (Trindade) channel, which has a depth of 200–400 m and width of up to 20 km. This channel runs in the WNW–ESE direction at a depth range of 4200–5000 m [*Faugères et al.,* 2002; *Lima et al.,* 2009]. The Rio de Janeiro channel has much smaller dimensions. This channel is oriented in the W–E direction and linked to the Rio de Janeiro fracture zone [*Bassetto et al.,* 2000; *Gonthier et al.,* 2003]. The largest tributaries are the Maçae channel running along the foot of the Almirante Saldanha Seamount and the Carioca channel, which is located southward (Figure 1A).

In this paper, the area between the Almirante Saldanha and São Tomé Seamounts, and the Vitoria-Trindade Seamounts and Maçae channel are studied (Figure 1B). According to the seismic data, the thickness of sediments deposited since the late Cretaceous on the continental rise of the southwestern Brazil Basin is 1–1.8 s TWT (two way time). The upper Pliocene–Quaternary seismic unit has a thickness of less than 0.1 s TWT [*Barker et al.,* 1983; *Lima et al.,* 2009; *Viana et al.,* 2003]. The Quaternary section recovered at DSDP site 515 located north of the northern Vema channel outlet (Figure 1A) is approximately 40-m-thick [*Barker et al.,* 1983]. It is composed of grayish brown terrigenous mud and clay with occasional nannofossil-rich layers and some foraminifer-rich layers [*Barker et al.,* 1983].

East of the São Tomé Seamount (core V14-13, 21°57′ S, 36°15′ W, water depth 4259 m, core length 6.56 m, 1957) sediments are presented by clay with thin laminas and wavy lenses of fine grained sand in the upper 1.88 m and yellowish brown to gray sand below (Lamont-Doherty Core Repository (LDCR)). South of the study area (core V24-254, 22°58′ S, 36°43′ W, water depth 4029 m, core length 5.73 m, 1967; core

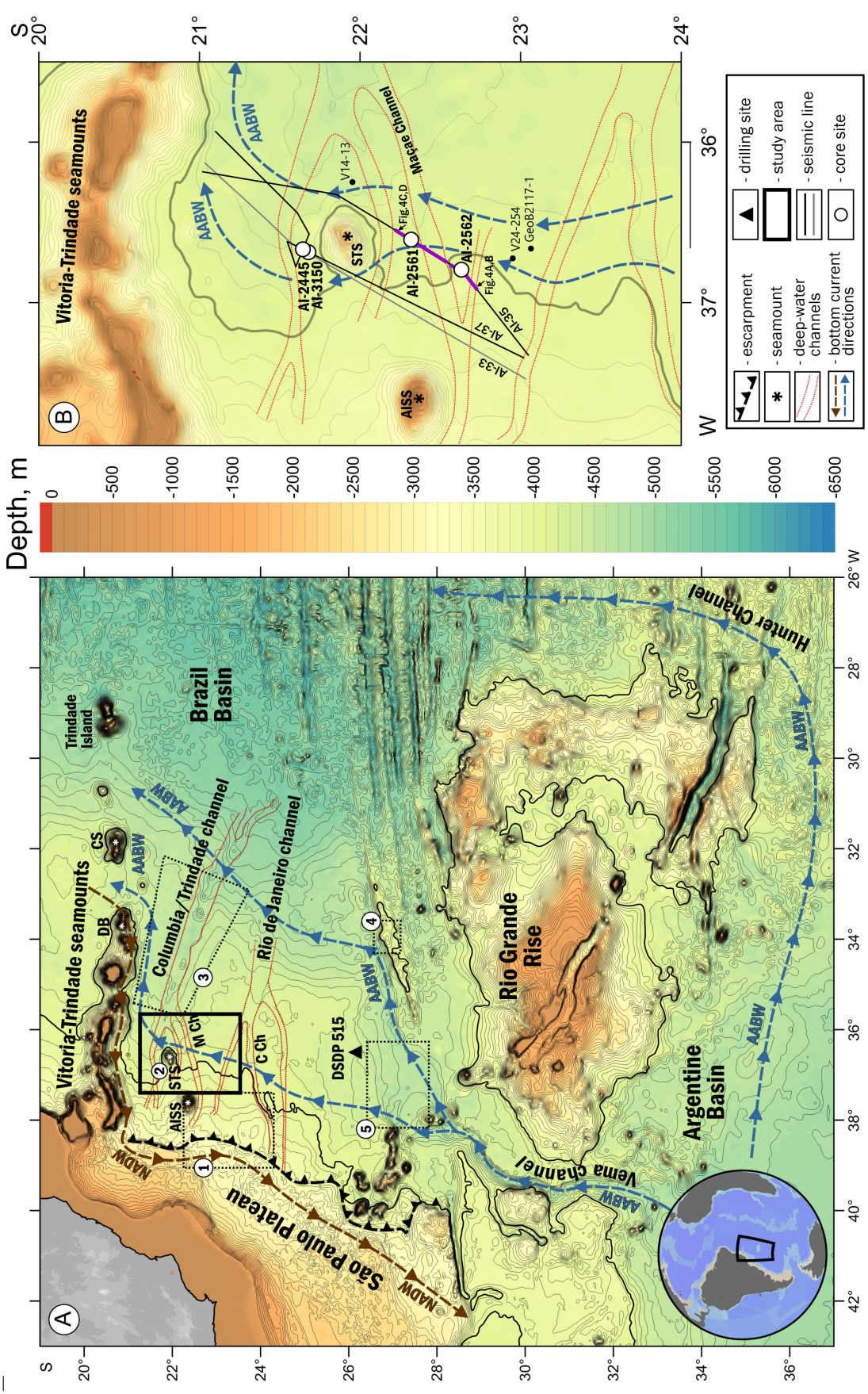

Figure 1. (a) Bathymetric map of the South Brazilian continental margin with directions of AABW and NADW currents, location of DSDP 515 drilling site and locations of main contourite, turbidite and mixed sedimentary systems (1 – São Tomé turbidite system [*Viana et al., 2003*; *Gonthier et al., 2003*]; 2 – São Tomé Seamount mixed system [*Borisov et al., 2013*]; 3 – Columbia channel mixed contourite-turbidite system [e.g., *Lima et al., 2009*]; 4 – Ioffe contourite drift [*Ivanova et al., 2016*]; 5 – Vema contourite fan [*Mézerais et al., 1993*; *Massé et al., 1994*]; AISS – Almirante Saldanha Seamount; DB – Dogaressa Bank; CS – Columbia Seamount; M Ch – Maçae channel; STS – São Tomé Seamount); (b) Regional seafloor topography of the study area with direction of the AABW current and location of cores and seismoacoustic profiles. Bold purple lines indicate fragments of seismic profile AI-35 shown in Figure 4.

GeoB 2117-1, 23°02.3′ S, 36°39, 1′ W, water depth 4045 m, core length 4.66 m, 1993) sediments consist of foraminiferal clay with sandy interbeds. Most of the sandy layers occur with homogenous structure, whereas sandy foraminiferal ooze layers are characterized by intense crossbedding (core V24-254) [*Bleil et al.,* 1993], LDCR.

1.2. Regional Oceanography

Bottom circulation in the deepwater part of the southwestern Brazil Basin is generally controlled by the Antarctic bottom water (AABW). The term AABW in this paper comprises the Weddell Sea deep water and lower part of the circumpolar water described by *Reid et al.* [1977].

The AABW propagates from the Argentine Basin to the Brazil Basin mainly through the Vema channel and Hunter channel, located east of the Rio Grande Rise (Figure 1A). Northward flowing bottom currents of Antarctic water move to the east along the Vitoria-Trindade chain and pass through the deep passages between the Dogaressa Bank, Columbia Seamount and Trindade Island [*Frey et al.,* 2019; *Morozov et al.,* 2010]. Modern AABW current velocities do not exceed 10 cm/s in the open basin, while in the channels and transform fault valleys, the current velocities exceed 20 cm/s [e.g. *Morozov et al.,* 2018].

The AABW is overlaid by highly saline, oxygen-rich and nutrient poor North Atlantic deep water (NADW), which flows south at a velocity of less than 5 cm/s [*Reid,* 1989, 1996]. A boundary between the AABW and NADW in the southern Brazil Basin corresponds to a depth of approximately 3600–3800 m and correlates with a neutral density isosurface of $\gamma^n = 28.16$ g/cm^3 [*Morozov et al.,* 2010].

1.3. Paleoceanographic Setting

The modern regime of oceanic sedimentation in this part of the western South Atlantic started during the Aptian/Albian (113 Ma, *Chang et al.* [1992]. The Late Cretaceous–Eocene sedimentation was likely dominated by hemipelagic settling and turbidity currents. The opening of the Drake and Tasman oceanic seaways in the Southern Hemisphere during the Eocene–Oligocene [e.g., *Allen and Armstrong,* 2008] caused dramatic changes in the ocean circulation. Since that time, deposition has been controlled by the interplay between geostrophic contour currents (along slope processes), gravity flows and mass-wasting processes from the continental slope and seamounts (downslope gravity driven processes). Global climate changes and tectonic movements resulted in a dramatic increase in NADW and AABW production, which caused episodes of drastic erosion and formation of several major regional unconformities. These unconformities represent time lines of the period from the Eocene–Oligocene to the late Pliocene [*Gamboa et al.,* 1983; *Faugères et al.,* 2002; *Lima et al.,* 2009; *Viana et al.,* 2003]. Lateral sedimentation processes are responsible for the formation of several depositional systems (Figure 1A): the São Tomé turbidite system at the foot of the São Paulo Plateau escarpment [*Gonthier et al.,* 2003; *Viana et al.,* 2003], Columbia channel mixed contourite-turbidite system (e.g., *Lima et al.,* 2009; *Murdmaa et al.,* 2012], São Tomé Seamount mixed system [*Borisov et al.,* 2013], Vema contourite fan [*Mézerais et al.,* 1993; *Massé et al.,* 1994] and Ioffe contourite drift [*Ivanova et al.,* 2016]. In this area, most of the channels transported sands during the Late Quaternary and remained active until recently [*Machado et al.,* 1998; *Viana et al.,* 1998].

2. Materials and Methods

This study is based on seismic, lithological and micropaleontological data acquired during cruises 33, 35, 37 and 43 of the RV *Akademik Ioffe* (2010–2013) [*Levchenko and Murdmaa,* 2013a, 2013b; *Levchenko et al.,* 2014; *Skolotnev et al.,* 2018] as well as publicly available bathymetric data.

2.1. Bathymetry

The physiographic map of the Brazil oceanic margin (scale 1 : 1, 883, 927) is used as the geomorphological background for the study area. This map was prepared by the Navy Center of Hydrography of the Brazil Directorate of Hydrography and Navigation, and the map comprises LEPLAC data (Brazilian Continental Shelf Survey Plan), nautical charts, ETOPO global relief model and General Bathymetric Chart of the Oceans–GEBCO.

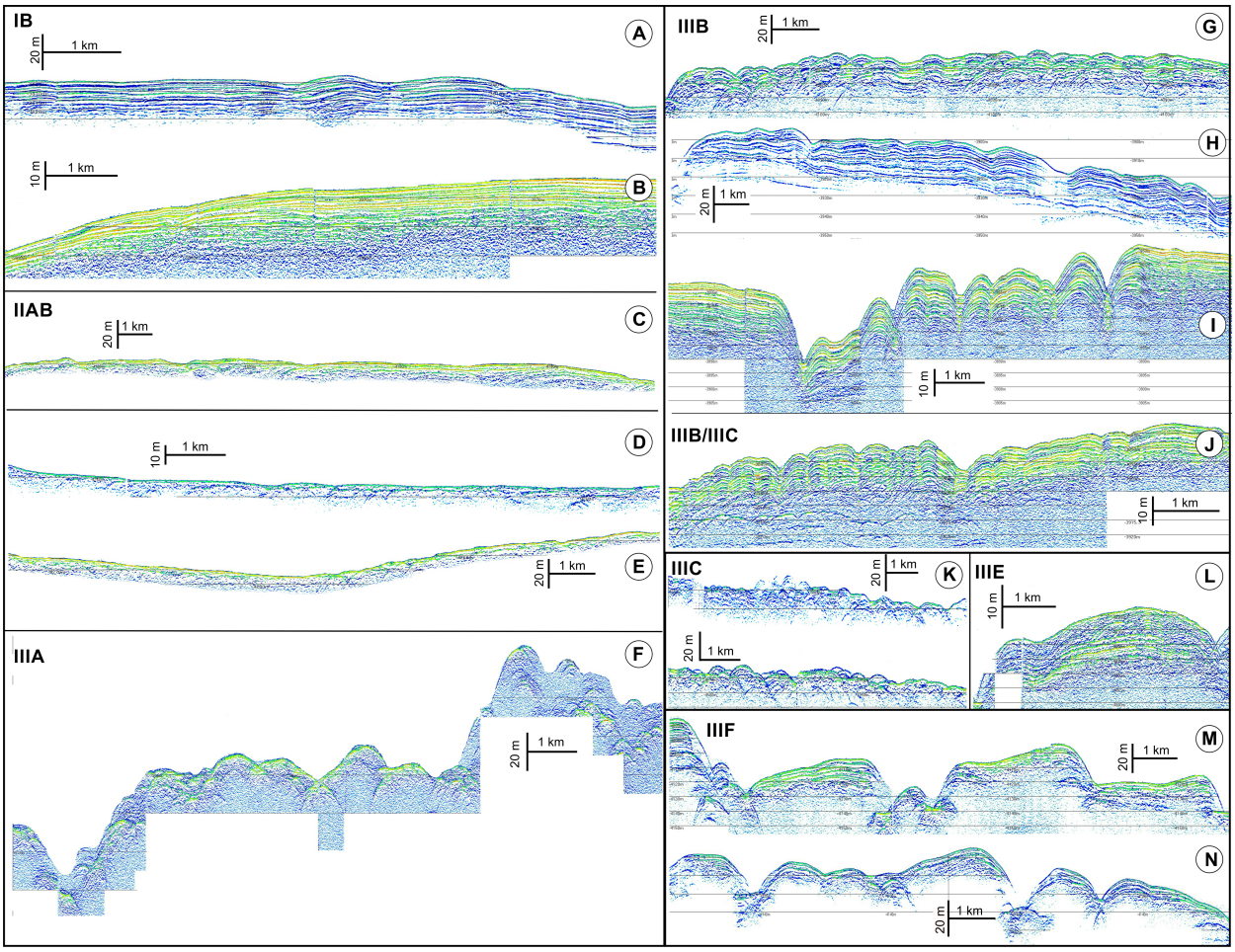

Figure 2. Seismic facies types distinguished in seismic sections (based on classification by *Damuth and Hayes* [1977]).

2.2. Seismic Profiling

High-resolution seismic lines running in the SW–NE direction east and west of the São Tomé Seamount were collected using the SES 2000 deep (Innomar Technologie GmbH, Germany) parametric sub-bottom echo-sounder (central frequency 4–5 kHz). Several short intersecting profiles were collected at the foot of the northwestern slope of the São Tomé Seamount. The acoustic penetration into the sediments reached 20–30 m with a vertical resolution of approximately 40 cm. Processing of the SES 2000 deep data was conducted using Interactive Sediment Layer Editor (ISE) software. A sound velocity of 1500 m/s was assumed for both the water column and sediments.

The profiles underwent seismic facies analysis, with the aim to determine the geometries of studied depositional features and their internal acoustic structures. A number of classifications of acoustic facies (also referred to as echofacies, echo character types, echos, and seismic facies in some cases) was developed during the last 45 years [*Damuth,* 1975, 1980; *Damuth and Hayes,* 1977; *Loncke et al.,* 2009; *Maestro et al.,* 2018; *Pratson and Laine,* 1989]. In this study, the echo character types are classified according to *Damuth* [1975, 1980], *Damuth and Hayes* [1977] and *Loncke et al.* [2009], mostly because these works are based on the data collected on the South American margin.

Since the acoustic images of the same deposits recorded using the SES 2000 deep profiler and echosounders in the 1960–70s differ due to their technical characteristics, the classification of seismic facies given by by *Damuth* [1975, 1980], *Damuth and Hayes* [1977] and *Loncke et al.* [2009] has been adapted for seismic facies distinguished in the SES 2000 deep records (Figure 2). This adaptation is based on a correlation between the SES 2000 deep

Table 1. Core Location

Core number	Latitude	Longitude	Water depth, m	Core length, m
AI-2445	21°38.3' S	36°40.1′W	4108	2.2
AI-2561	22°18.8′ S	36°35.8′ W	4053	1.94
AI-2562	22°37.8′ S	36°47.5′ W	3950	3
AI-3150	21°40.237′ S	36°41.178′ W	4090	2.61

seismic data collected during cruises 32, 33, 35, 37, and 40 of the RV *Akademik Ioffe* (2010–2013) in the Western Atlantic [*Levchenko and Murdmaa,* 2013a, 2013b; *Levchenko et al.,*2014] and the seismic facies distribution map of the east Brazilian oceanic margin, which was published by *Damuth and Hayes* [1977]. In the seismic records collected using the SES 2000 deep profiler, distinguishing facies type IIA from IIB is difficult, and thus, these types were combined into type IIAB (Figure 2C–Figure 2E), which is described further in detail.

2.3. Lithology

Four gravity cores with recoveries from 1.94 to 3 m were retrieved to the northwest and southeast of the STS at water depths from 3950 to 4108 m (Figure 1A, Figure 1B). The coordinates, water depths, and core lengths of each core are provided in Table 1. All collected cores were subjected to visual macroscopic and smear-slide descriptions. After opening, the hue and chroma attributes of the sediment color were determined using the Munsell Geological Rock Color Chart [*Munsell Color Company,* 1995].

Geochemical and grain-size analyses were carried out in the Atlantic Branch of the Shirshov Institute of Oceanology RAS. Calcium carbonate content ($CaCO_3$) were measured using the AN-7529 express coulometric carbon analyzer (Gomel Plant of Measuring Equipment, Republic of Belarus) on 94 dried sediment samples taken from all cores. Sampling intervals in homogenous layers were 15–30 cm and 2–3 cm in sand/silt rich or laminated layers.

Grain-size distribution analyses were performed with the SALD 2300 laser diffraction particle size analyzer (Shimadzu, Japan) on 119 bulk sediment samples taken from cores AI-2561, AI-2562, and AI-3150. This type of analysis was conducted every 10–30 cm in homogenous and bioturbated layers and every 1–2 cm in suggested gravitite or contourite cycles. The grain-size distribution of the terrigenous fraction was studied in samples from the same intervals after removal of $CaCO_3$ by an HCl N1 solution. Samples for the analyses were dispersed by ultrasonation in sodium tripolyphosphate solution.

Volume magnetic susceptibility was measured on split cores (AI-2561, AI-2562, and AI-3150) using the Bartington MS3 meter and Bartington MS2E surface sensor. Measurements were performed at 0.5 cm intervals. Core AI-2445 was not subjected to magnetic susceptibility measurements due to a lack of an archive half of the core.

2.4. Micropaleontology

The pilot study of foraminiferal assemblages, index species and fragmentation (the ratio of fragments to the sum of fragments and whole tests) was performed under the MBI6 binocular at grain-size fractions of > 0.1 mm. The sampling interval ranged from 5 to 45 cm depending on the sediment lithology and $CaCO_3$ content.

3. Results

3.1. Seismic Profiling

The seismic facies analysis revealed two widespread types of seismic facies in the study area: IB and IIAB. Type IB facies are characterized by continuous, sharp, parallel moderate-amplitude reflectors persisting for tens of kilometers and an acoustic penetration of approximately 15–30 m (Figure 2A, Figure 2B). These facies are traced

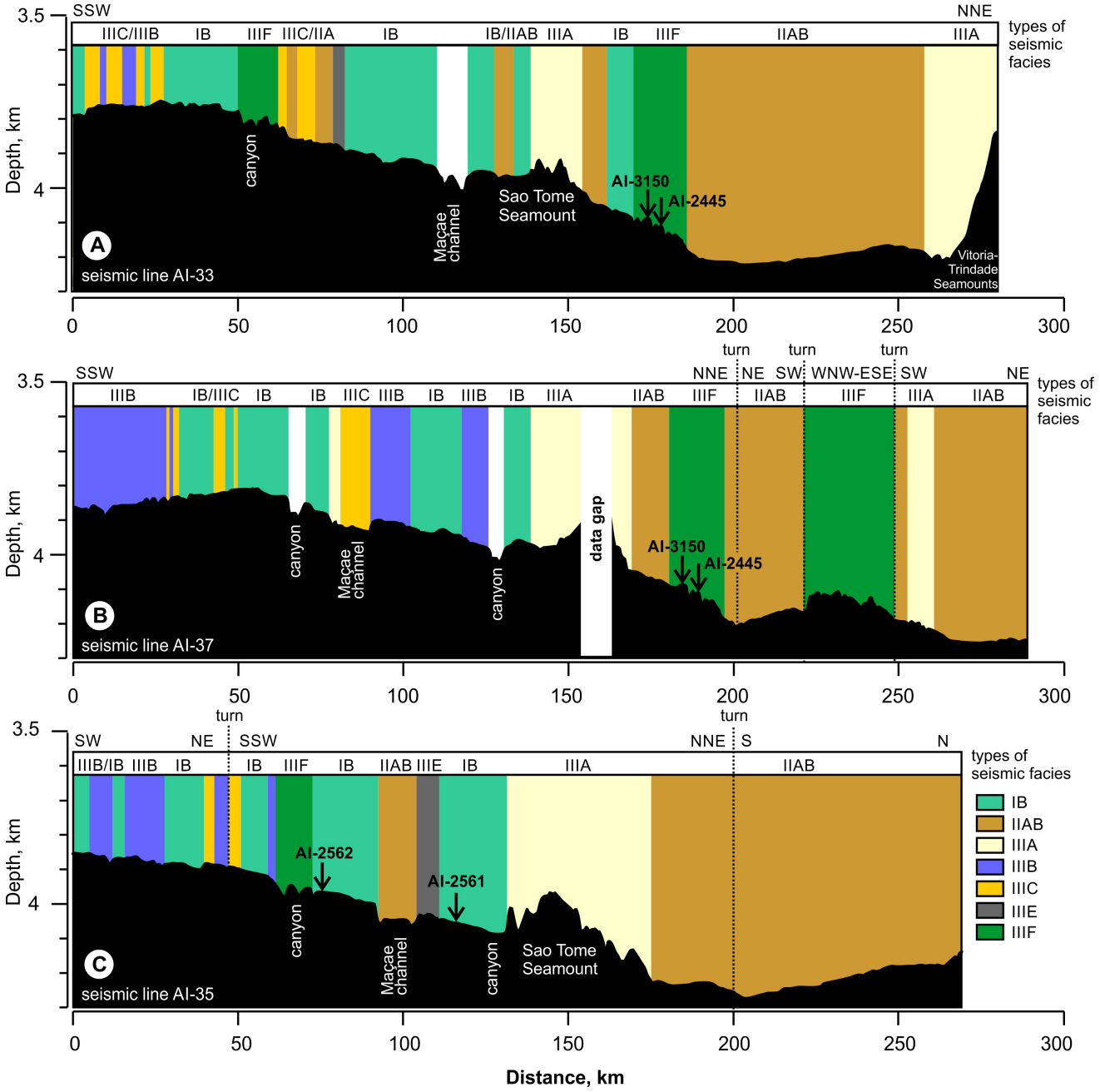

Figure 3. Seismic facies distribution along the SES 2000 deep seismic lines with locations of sediment cores (black arrows). Location of seismic lines is shown in Figure 1B.

south of the São Tomé Seamount and at the foot of its western slope. Seismic facies of type IIAB show intermittent parallel moderate to high-amplitude reflectors with zones characterized by the absence of sub-bottom reflectors. Acoustic penetration varies from 5 to 15 m (Figure 2C–Figure 2E). These facies are widespread north of the São Tomé Seamount and are found in the Maçae channel valley (Figure 3). The widths of the Maçae channel in the upper part reaches 18 km and its relative depths is approximately 40–45 m. The other channels crossed by seismic lines are smaller and did not exceed 7 km in width and 40 m in depth. Large, irregular, overlapping and single hyperbolae with widely varying vertex elevations above the sea floor correspond to type IIIA facies (Figure 2F), which are related to the São Tomé Seamount and Vitoria-Trindade chain.

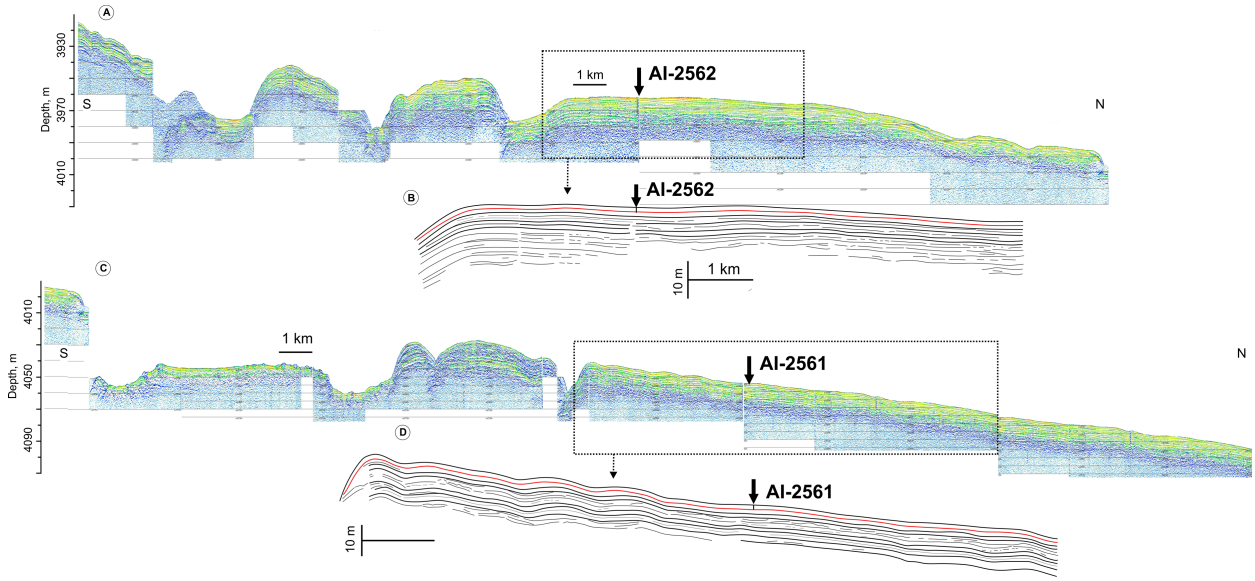

Figure 4. Fragments of seismic profile AI-35 (with interpretation). Red solid line indicate seismic reflector corresponding to coarse grained layer recovered in the lower parts of the sediment cores. Location of seismic lines and core is shown is Figure 1B. Core lithology is presented in Figure 6.

Type IIIB is characterized by regular, single or slightly overlapping hyperbolae with conformable reflectors (acoustic penetration of 20–25 m). These facies are generally traced in areas adjacent to channels. The height of the hyperbolae varies from 5 to 15 m and the wavelength is approximately 0.2–1 km (Figure 2G–Figure 2I). Most of these wave-like features demonstrate migration toward the nearest channel. Overlapping hyperbolae with varying vertex elevations above the sea floor and no sub-bottom reflectors related to type IIIC were found in the Maçae channel valley or alternating with the IIIB facies (Figure 2J, Figure 2K). Seismic facies IIIE represent zones of regular, intense, overlapping hyperbolae with vertices tangent to the sea floor, which are interrupted by zones of distinct echoes with parallel sub-bottom reflectors (Figure 2L). These facies are related to the northern slope of the Maçae channel. South of this channel and northwest of the São Tomé Seamount, the seismic lines crossed broad, single, irregular hyperbolae with disconformable reflectors and acoustic penetrations of 10–20 m (type IIIF facies) (Figure 2M, Figure 2N).

Sediment cores AI-2561 and AI-2562 were collected in the distribution area of seismic facies type IB (Figure 3C). Acoustic penetration in this area is 25 m. The uppermost sub- bottom reflector was identified at depths of approximately 2–3 m below sea floor (BSF) (Figure 4). Cores were retrieved from sites AI-2445 and AI-3150 in the distribution area of seismic facies type IIIF (Figure 3A, Figure 3B). The cores were retrieved from mounded sediment bodies with relative heights of 15–25 m separated by small channels. Depositional bodies with evidence of migration toward the channels are related to their northern gentle flanks, while bodies with evidence of erosion are adjacent to steep southern flanks. Acoustic penetration in this area varies from 5 to 20 m. The two uppermost seismic reflectors were identified at water depths of 1 and 2 m BSF, respectively (Figure 5).

3.2. Lithology

From core AI-2562, intercalations of bioturbated, foraminifera-bearing, clayey silt layers and nearly pure terrigenous silt and clayey silt layers with sandy silt/silty sand interbeds of several millimeters thickness were recovered (Figure 6, Figure 7A, Figure 7I). The carbonate content varies from 1.6 to 33%. In the lower part of the core, there is 5-cm-thick layer of well-sorted sand, which is gener-

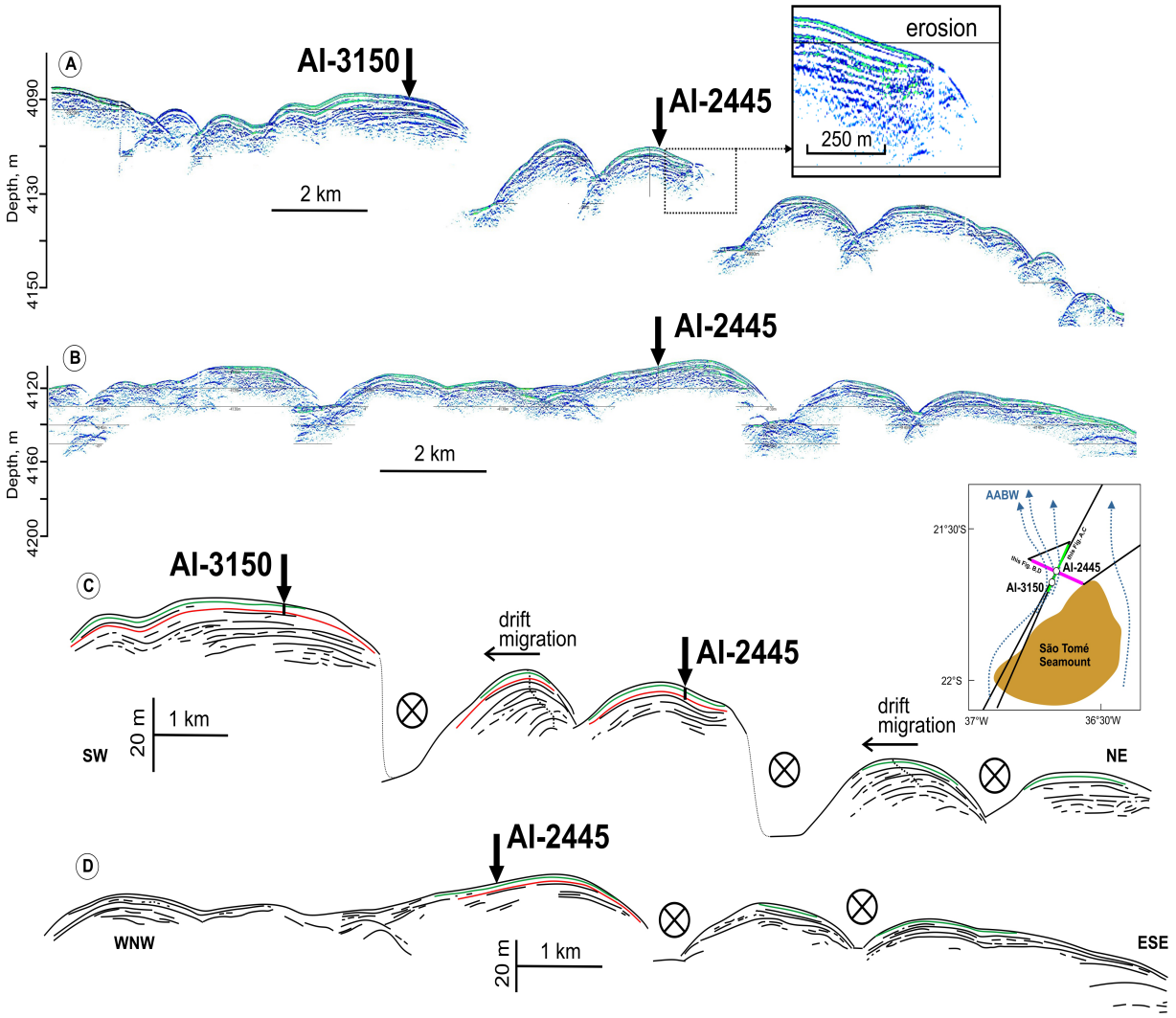

Figure 5. Fragments of seismic profile AI-37 (with interpretation). Red solid line indicates seismic reflector corresponding to coarse grained layer recovered in the lower parts of the sediment cores. Green solid line marks seismic reflector corresponding to the layer of foraminiferal sand in cores AI-3150 and AI-2445. Seismic evidence of erosion is presented in the upper right insert. Suggested direction of bottom currents near the São Tomé Seamount is shown in the lower right insert. Location of seismic lines is shown is Figure 1B. Core lithology is presented in Figure 6.

ally composed of quartz and feldspar (Figure 7F). Numerous burrows of benthic fauna are scattered throughout the interval, and upper and lower contacts of the layer are distinct but disturbed by bioturbation. The coarse-grained layer overlies a silt-sand-enriched layer with lenses of well-sorted sand. A grain-size analysis showed reverse grading in the layer with sand lenses and normal grading with unimodal distribution in the sand layer. The grain size distribution in the layer with sand lenses demonstrate bimodal distribution with peaks related to sand and clay.

Core AI-2561 is represented by intercalation of yellowish-brown silt and clayey silt with an admixture of nannofossils, foraminifera and their fragments. Carbonate content is generally low, ranging from 3 to 30%. Thin lenses of sandy silt with a thickness of approximately 5–8 mm were revealed

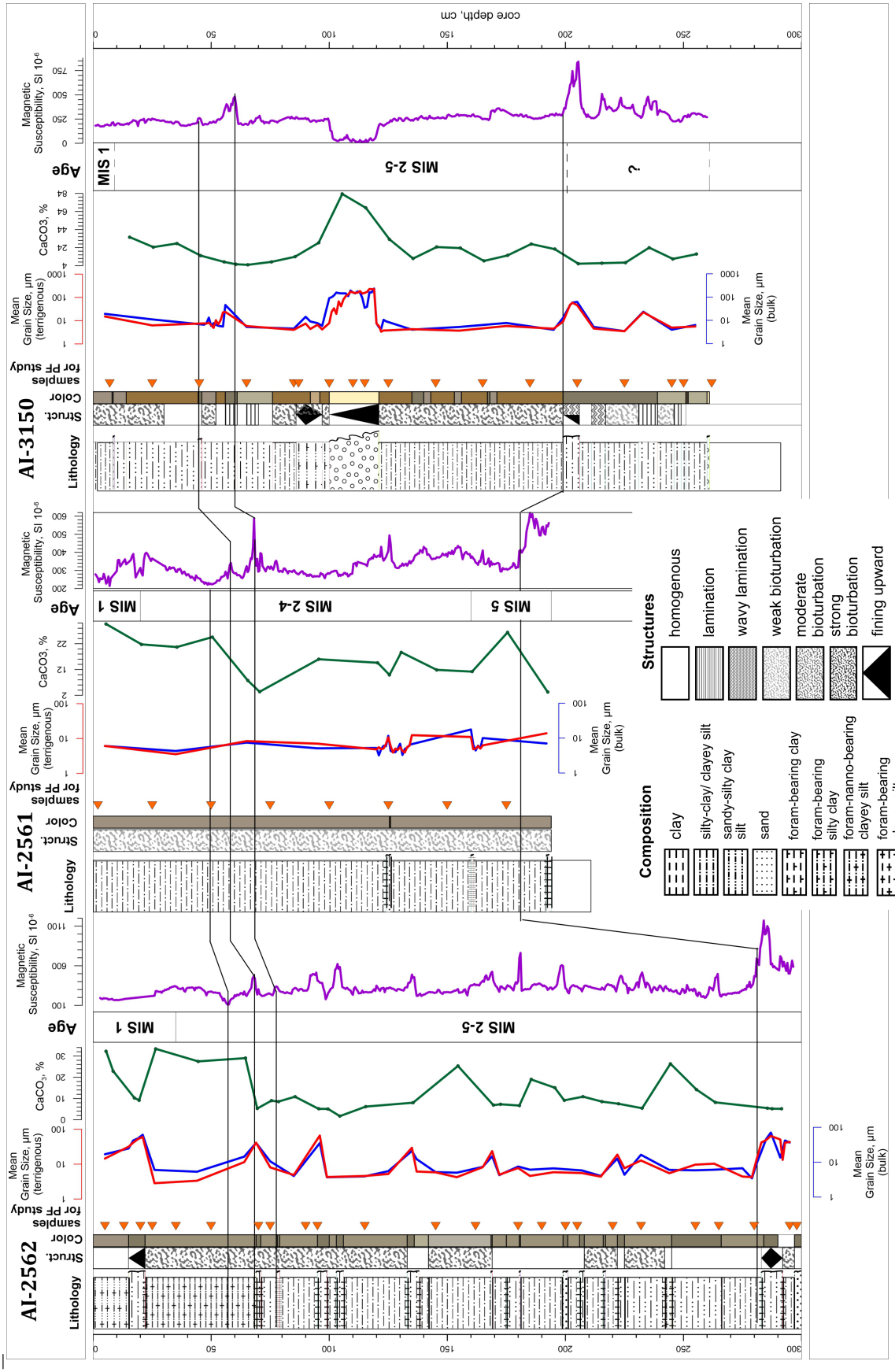

Figure 6. Lithology, calcium carbonate content, mean grain size (for bulk sediment and terrigenous fraction after removal of $CaCO_3$), magnetic susceptibility and age of sediments recovered from cores. Black solid lines mark correlation between sediment cores. Orange circles indicate sampling intervals for foraminiferal study. PF – planktic foraminifera. Location of cores is shown in Figure 1B.

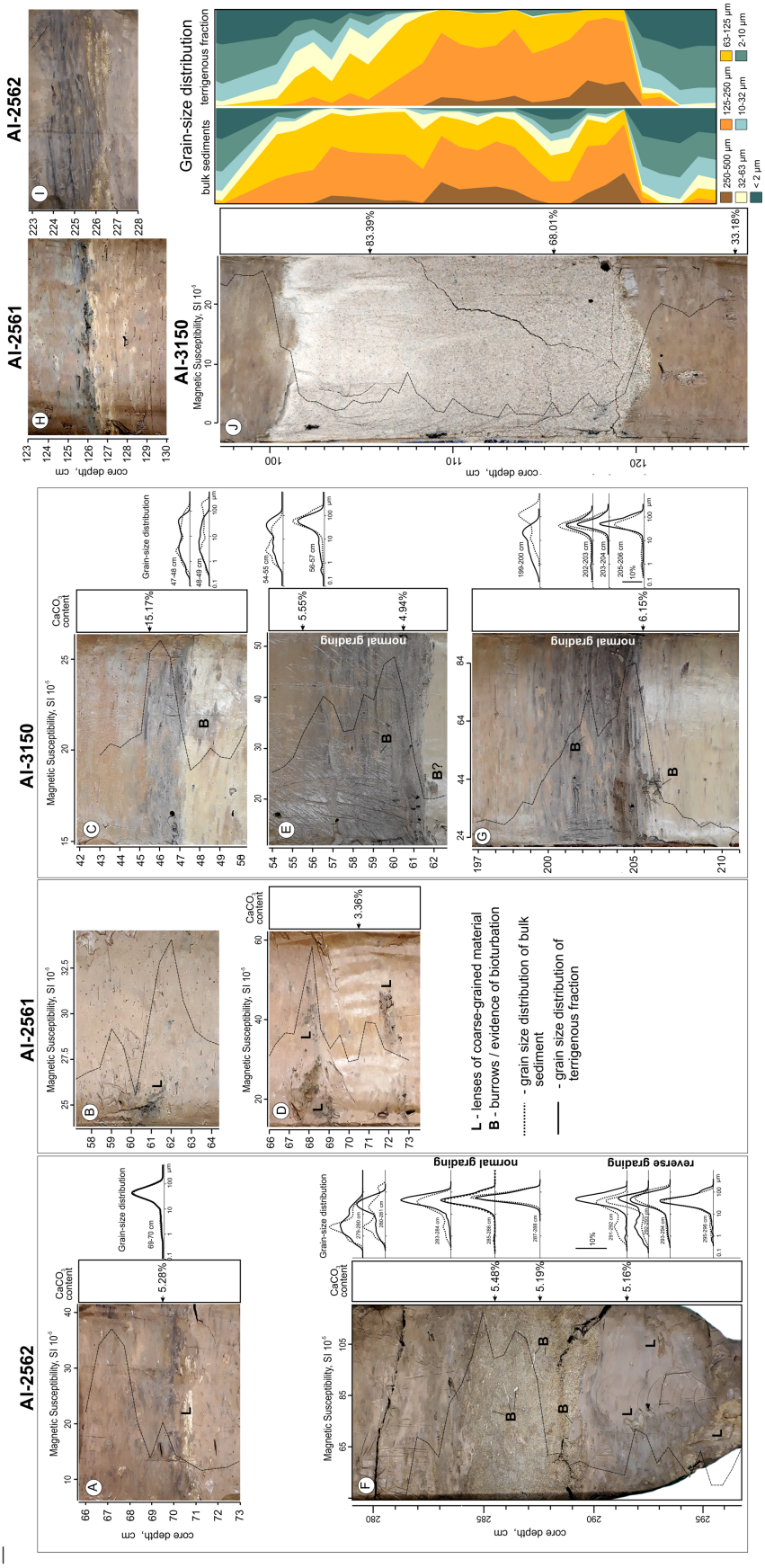

Figure 7. Photos of split core fragments with evidence of lateral sedimentation. Black dashed lines on photos indicate variations in magnetic susceptibility. Black arrows mark intervals with measured carbonate content. Grain-size distributions are shown right of the photos. Color of sediments is changed due to oxidation. Location of cores is shown in Figure 1B.

at core depth intervals of 58–63 cm, 66–73 cm, and 124–126 cm (Figure 7B, Figure 7D, Figure 7H). Sand was found in the core catcher.

Recovered from cores AI-3150 and AI-2445 were bioturbated, yellowish-brown clayey silt and foraminifera-bearing clayey silt with three 5 to 7-cm-thick sand-enriched intervals (Figure 7C, Figure 7E, Figure 7G) and a layer of foraminiferal sand (21-cm-thick in core AI-3150 and 16-cm-thick in core AI-2445 [*Murdmaa et al.,* 2012] with a significant amount of quartz (Figure 7J). Sand-enriched intervals demonstrate normal grading (slight decrease in in mode value of the grain size distribution toward the core top) and strong evidence of bioturbation, even in basal layers. A distinct, normal grading was distinguished for a terrigenous fraction of the foraminiferal sand layer. A grain-size analysis of bulk sediment samples showed moderately well-sorting in the upper part of the foraminiferal sand layer (103–111 cm). As for the terrigenous fraction in the upper half of the layer, quartz grains are poorly-sorted, whereas in the lower half, sediments are moderately to well-sorted (Figure 7J).

Silt and sand-enriched layers revealed in cores are generally darker than the over and underlying sediment (Figure 7A, Figure 7H, Figure 7I). In some cases, these layers demonstrate parallel lamination (distinct or partly destroyed by bioturbation). Thin layers and lenses of fine sand were observed at the base of most laminated layers. Coarse-grained layers correspond to the highest values of magnetic susceptibility (Figure 7C–Figure 7G). The lowest values correspond to foraminiferal sand layers (Figure 7J).

3.3. Foraminiferal Study

In all four cores, planktic foraminiferal fauna of tropical-to-subtropical character demonstrate downcore variations in preservation and diversity. The cores comprise Late–Middle Quaternary foraminiferal assemblages with index species *G. ruber* pink and *G. truncatulinoides*. The intervals with better preservation generally contain specimens of the *G. menardii* group. However, there are rare and sporadic occurrences of reworked Neogene species in all cores, including *Globorotalia multicamerata*, *Dentoglobigerina altispira, Pulleniatina primalis, Globorotalia miocenica, G. exilis, G. margaritae*, and others.

Benthic foraminifera occur in low numbers in nearly all core samples. These foraminifera are represented by several species including *Cibicides wuellerstorfi, Oridorsalis umbonatus, Pullenia bulloides, and Nuttalides umbonifer*. The former three taxa are known to be associated with NADW, whereas the last taxa is considered to be typical of AABW [*Harloff and Mackensen,* 1997; *Mackensen et al.,* 1993]. A clear relationship between glacial and interglacial stratigraphic intervals and the occurrence of specific benthic assemblages or species was not found in any of the cores studied.

The upper interval (0–20 cm) of core AI-2561 contains a tropical planktic foraminiferal assemblage of medium preservation (fragmentation 30–50%) with aforementioned species of *Globigerinoides ruber* pink, *Globorotalia trancatulinoides* and *Globorotalia menardii*. The underlying interval (20–160 cm) is characterized by a strong fragmentation (up to 90–95%), decrease in species diversity, increase in faunal portion of dissolution resistant species (such as *Globorotalia inflata, Globigerinoides conglobatus* and *Pulleniatina finalis*) and an absence of *G. menardii* group. The fauna in the lowest analyzed sample (175 cm) is similar to those in the uppermost interval.

There is a similar foraminiferal fauna, notably in the upper 35 cm, that is generally more abundant and better preserved in shallow-water core AI-2562 than in core AI-2561. However, foraminiferal dissolution is also significant in core AI-2562. The interval (35–300 cm) demonstrates a downcore increase in fragmentation. The index species *G. ruber* pink occurs only in the upper 75 cm. However, the absence of this species in the lower part of the core is most likely the result of stronger dissolution. The *G. menardii* group occurs in significant numbers in the warm water assemblages in the upper 35 cm and at 252 cm, is the broken specimens of the same group are found at 145 cm and from the intervals 35–50 cm and 200–300 cm. In the latter interval, several tests of *G. menardii-tumida flexuosa* are found.

In cores AI-2445 and AI-3150, downcore changes in preservation and an alternation between more and less warm water assemblages are inferred. The turbidite layers in both cores are especially rich in the foraminiferal tests including the reworked specimens of Neogene species.

4. Discussion

4.1. Stratigraphy

The strong dominance of extant foraminiferal species, including *Globigerinoides ruber* pink and *Globorotalia truncatulinoides* in all examined samples of the four cores suggests the recovered sediments are of Quaternary age, regardless of the rare occurrence of reworked Neogene species. In the nearby area of the Rio Grande Rise and the Ioffe Drift, *G. ruber* pink is typical of the last 280 ka and *G. truncatulinoides* occurred during the last 1.8–2 Ma [*Barash et al.,* 1983; *Ivanova et al.,* 2016, and references therein). The intervals with better preservation generally contain specimens of the *G. menardii* group, which are typical of interglacials in the Atlantic [*Ericson and Wollin,* 1968]. Hence, the presence/absence of the *Globorotalia menardii* group as well as changes in foraminiferal preservation and $CaCO_3$ content collectively suggest that cores AI-2561 and AI-2562 most likely covered the last climatic cycle (MIS 5.5-1). In addition, an occurrence of *G. menardii-tumida flexuosa* is indicative of the last interglacial (MIS 5.5) in the Atlantic [e.g., *Barash,* 1988]. If the assumption about the Late Quaternary age of both cores is correct, a mean sedimentation rate of approximately 1.6 and 2 cm/ka can be estimated for cores AI-2561 and AI-2562, respectively. These estimates are in line with previously obtained values from core GeoB 2117-1 [*Bleil et al.,* 1993], which is located southward of core AI-2562 (water depth 4045 m). Unfortunately, the stratigraphic subdivision of cores AI-2445 and AI-3150 is hampered by the occurrence of at least two turbidite layers.

Along with foraminiferal data the recovered sections were correlated based on magnetic susceptibility records and lithological data. A correspondence found between the coarse-grained sedimentary sequences found in each core suggests that the upper 198 cm of core AI-3150 also covered the last climatic cycle (MIS 5.5-1).

4.2. Seismic and Lithological Evidence of Lateral Sedimentation

The prevalence of seismic facies IIAB corresponding to coarse-grained deposits confirms a previous suggestion [*Faugères et al.,* 2002; *Lima et al.,* 2009] about the domination of gravity driven sedimentation processes north of the São Tomé Seamount. Gravity flows in this area transport coarse-grained material from the continental slope and Vitoria-Trindade Seamounts to the continental rise.

A diversity of seismic facies south of the São Tomé Seamount suggests a complicated interplay between different sedimentation processes (Figure 3). Seismic facies type IIIB usually corresponds to contourite features [e.g. *Damuth and Hayes,* 1977]. However, in the case of the study area, it is difficult to define the sedimentation processes responsible for formation of these wave-like depositional features. The study area is affected by gravity flows moving from the continental slope through the widespread network of canyons and channels.

As postulated by *Embley et al.* [1980], the curvature of hyperbolic echoes depends on the angle between the ship's heading and the actual bedforms: the hyperbolae are the steepest when a seismic line runs normal to the sediment wave orientation. Based on the configuration of the recorded, well-defined sediment waves, these features may be oriented both normal or at a small angle to seismic lines (and to the general direction of AABW current). The available data do not allow us to precisely distinguish the sediment wave orientation.

Domination of seismic facies type IB points to rather low bottom current velocity on a long-term scale out of prominent topographic obstacles (Figure 3). Nevertheless, current velocity can increase due to water flow overcoming obstacles. Internal waves may have been generated when the flow of bottom water crossed the described channels, which could also affect the formation of sediment waves. This mechanism was described by [*Hernández-Molina et al.,* 2008]. Furthermore, the simultaneous action of bottom currents and gravity flow might also be responsible for sediment wave formation. Alternation of seismic facies IIIC and IIIB as well as IIIC and IB could be considered evidence of post-depositional deformation or mass-wasting processes. Seismic facies IIIF south of the Maçae channel mark the embranchment of smaller channels running in the ESE direction (Figure 3). These facies at the foot of the northeastern slope of the São Tomé Seamount are related to the erosional-depositional system briefly described by [*Borisov et al.,* 2013]. This system consists of sev-

eral mounded depositional bodies with the sizes of approximately 1.9 km × 2.9 km, which are separated by small channels (Figure 5). According to the configuration of erosional and depositional features and the direction of the Coriolis force, the system was likely formed by the AABW bottom current along the western slope of the São Tomé Seamount. As a large topographic obstacle, the seamount increases the bottom current velocity. Due to the local bottom topography, several high velocity jets most likely occurred in the flow structure. These jets were rather stable in time and space and formed an erosional-depositional system at the base of the seamount.

Coarse-grained layers observed in the sediment cores are undoubtedly of turbiditic origin, but some of these layers might be affected (reworked) by bottom currents. Bioturbation and specific sediment structures, such as wavy layers at the base of laminated intervals and lenses of silt and sand, were considered to be criteria for distinguishing between contourites and turbidites [*Stow and Faugères,* 2008; *Wetzel et al.,* 2008]. Evidence of bioturbation can also occur in turbidites, but in some intervals of the studied cores, even basal sand-enriched layers were affected by bioturbation (Figure 7F, Figure 7E, Figure 7G). The bi-gradational sedimentary sequence recovered in the lower part of core AI-2562 contains strong evidence of bioturbation (Figure 7F) and can be generally described by a standard contourite facies model [*Hüneke and Stow,* 2008; *Stow and Faugères,* 2008]. The bi-gradational structure of the layer most likely resulted from long-term fluctuations in bottom current velocity. The foraminiferal sand layer in cores AI-2445 and AI-3150 corresponds to gravity flow (grain flow) deposits (Figure 7J). A considerable amount of quartz indicates that this material was derived from the continental slope. The largest amount of coarse-grained layers in core AI-2562 indicates that during the Late Quaternary, the gravity flow activity in the Maçae channel was higher than in the channels located northward. Due to the overspill of gravity flows resulting from a change in orientation of the Maçae channel, the transported sediment material was deposited on the southern flank of the channel (in the area of core AI-2562). The same mechanism most likely took place northward of the São Tomé Seamount in the area of cores AI-3150 and AI-2445.

A correlation between seismic lines and sediment layers showed that a prolonged reflector at 2–3 m BSF likely corresponds to the coarse-grained sedimentary sequence recovered in the lower parts of the cores (Figure 4, Figure 5). The foraminiferal sand layer corresponds to a reflector at a depth of approximately 1 m BSF. Thus, a previously described correlation between the seismic reflector and foraminiferal sand layer [*Borisov et al.,* 2013; *Murdmaa et al.,* 2012] is now confirmed for the depositional bodies at the foot of the northeastern slope of the São Tomé Seamount.

Most likely, hemipelagic settling through the water column did not play a significant role in sedimentation in the study area during the Late Quaternary. The sediments over and underlying the coarse-grained intervals resulting from turbidity flows and bottom current activity are generally composed of fine and medium silt (clay amount does not exceed 35%). The southwestern part of the Brazil Basin is characterized by a lack of large rivers, which would be able to produce large plumes and provide enormous amounts of silt material to the study area, as the nearest large river is more than 400 km from the shore. Additionally, this area is very distant from the La Plata River (∼ 2500 km) and Amazon River (∼ 3000 km), which are the main sources of fluvial material in the region. Thus, silt and sand material were transported to the continental rise by gravity flows. Silt enrichment in the major part of the recovered sediments together with an absence of turbidite evidence might be explained by bottom current activity, which washed out the clay material and reworked the gravity flow deposits.

According to the mentioned criteria for contourite identification, the coarse-grained sedimentary sequences corresponding to higher values of magnetic susceptibility and correlated with each other were interpreted as turbidites reworked by bottom currents. Notably, the sedimentary sequence shown in Figure 7E may represent a turbiditic sequence (only proposed bioturbation evidence in the basal layer suggests its contourite origin). The upper two sequences are related to low carbonate intervals corresponding to MIS2–MIS4. Sedimentary sequences in the lower parts of the cores correspond to MIS 5 (complete sequences were found only in cores AI-2562 and AI-3150, whereas in core AI-2561, sand material was found

in the core catcher). The formation of such coarse-grained layers should be linked to increased gravity flow activity and an intensification of bottom currents, which reworked the turbidite deposits. Variations in sea-level in response to glacial-interglacial cycles controlled the sediment supply in this area [e.g., *Lima et al.,* 2009]. A relationship between glacial-interglacial cycles and changes in the AABW velocity during the Quaternary is still a subject of discussion among researchers. Some authors suggest intensification of the AABW current during the transition from interglacial to glacial periods [*Ledbetter,* 1986; *Massé et al.,* 1994]. Alternatively, some researchers [e.g., *Ledbetter,* 1984; *Pudsey and Howe,* 1998] argue that the AABW current in the Atlantic reached its maximum velocity during the interglacial periods. Recent publications suggest an increase in the AABW intensity during the Last Glacial Maximum compared to the Holocene [*Spooner et al.,* 2018] The data presented in this paper do not distinctly solve this issue.

Downcore planktic foraminiferal preservation varies significantly in cores AI-2561 and AI-2562, which mainly reflects the well-known glacial-interglacial variations in lysocline depth associated with variations in AABW production. Low sedimentation rates in the study area might be explained by both low sediment supply typical of an arid climatic zone and by short-term hiatuses in the sediment record resulting from bottom current activity.

Conclusions

The São Tomé Seamount marks a boundary between two zones characterized by different sedimentation regimes. North of the seamount sedimentation is controlled by gravity flows, which transport material from the continental slope and Vitoria-Trindade Seamounts downslope to the Columbia channel. The São Tomé Seamount also plays an important role in the formation of erosional and depositional features at the base of the northwestern slope of the seamount. As a large topographic obstacle, the seamount causes an increase in the AABW current velocity and thus changes the AABW flow structure. The area south of the São Tomé Seamount is characterized by the resulting strong interaction between the gravity flows and AABW bottom current. This interplay resulted in the formation of bottom current reworked turbidites, which were recovered in the sediment cores. Seismic and lithological data indicate a domination of lateral sedimentation over hemipelagic settling in the study area during the last glacial-interglacial cycle at minimum. During this period, gravity flows were the most active in the Maçae channel. Intensification of gravity driven processes in the study area is most likely linked to sea-level low-stands during glacial periods. Variations in the AABW current velocity in response to glacial-interglacial climate changes during the Late Quaternary remain a subject for discussion.

Acknowledgments. The authors are grateful to scientific party, master and crew of RV *Akademik Ioffe* cruises 33, 35 and 37 for their professional assistance with seismic profiling and coring. The study was partially supported by the Russian Science Foundation grants 14-50-00095 (magnetic susceptibility measurements) and 18-17-00227 (seismic, sedimentological and micropaleontological studies and interpretations). The advanced English language editing was provided by the Wiley Editing Services.

References

Allen, M. B., H. A. Armstrong (2008), Arabia–Eurasia collision and the forcing of mid-Cenozoic global cooling, *Palaeogeography, Palaeoclimatology, Palaeoecology, 265,* No. 1–2, 52–58, **Crossref**

Barash, M. S. (1988), *Quaternary Paleooceanology of the Atlantic Ocean*, Nauka, Moscow. (in Russian)

Barash, M. S., N. S. Oskina, N. S. Bylum (1983), Quaternary Biostratigraphy and Surface Paleotemperatures Based on Planktonic Foraminifers, *Initial Reports of the Deep Sea Drilling Project, 72 (eds. P. F. Barker, D. A. Johnson, & R. L. Carlson)* p. 849–869, U.S. Government Printing Office, Washington. **Crossref**

Barker, P. F., D. A. Johnson, R. L. Carlson, et al. (1983), Site 515: Brazil Basin, *Initial Reports of the Deep Sea Drilling Project, 72 (P. F. Barker et al. (eds.)* p. 54–154, U.S. Government Printing Office, Washington.

Bassetto, M., F. F. Alkmim, et al. (2000), The oceanic segment of the Southern Brazilian margin: Morpho-structural domains and their tectonic significance, *Geophysical Monograph Series*, *115,* 235–299.

Bleil, U., M. Breitzke, H. Buschhoff, et al. (1993),

Report and preliminary results of Meteor Cruise 23/2, Rio de Janeiro-Recife, 27.02.–19.03.1993, *Berichte, Fachbereich Geowissenschaften, Universität Bremen*, No. 43, 133.

Borisov, D. G., I. O. Murdmaa, E. V. Ivanova, et al. (2013), Erosion – Accumulative Activity of the Bottom Currents on the Continental Rise of Brazil, *Doklady Earth Sciences*, *452,* No. 3, 979–982, **Crossref**

Chang, H. K., R. O. Kowsmann, A. M. F. Figueiredo, A. Bender (1992), Tectonics and stratigraphy of the East Brazil Rift system: an overview, *Tectonophysics*, *213,* No. 1–2, 97–138, **Crossref**

Damuth, J. E. (1975), Echo character of the western equatorial Atlantic floor and its relationship to the dispersal and distribution of terrigenous sediments, *Mar. Geol.*, *18,* 17–45, **Crossref**

Damuth, J. E. (1980), Use of high-frequency (3.5–12 kHz) echograms in the study of near-bottom sedimentation processes in the deep-sea: A review, *Mar. Geol.*, *38,* 51–75, **Crossref**

Damuth, J. E., D. E. Hayes (1977), Echo character of the East Brazilian continental margin and its relationship to sedimentary processes, *Marine Geology*, *24,* No. 2, 73–95, **Crossref**

Embley, R. W., P. J. Hoose, P. Lonsdale, L. Mayer, B. E. Tucholke (1980), Furrowed mud waves on the western Bermuda Rise, *Geological Society of America Bulletin*, *91,* No. 12, 731, **Crossref**

Ericson, D. B., G. Wollin (1968), Pleistocene Climates and Chronology in Deep-Sea Sediments, *Science*, *162,* No. 3859, 1227–1234, **Crossref**

Faugères, J.-C., A. F. Lima, L. Massé, S. Zaragosi (2002), The Columbia Channel-levee system: a fan drift in the southern Brazil Basin, *Geological Society, London, Memoirs*, *22,* No. 1, 223–238, **Crossref**

Frey, D. I., E. G. Morozov, I. Ansorge, et al. (2019), Thermohaline structure of Antarctic Bottom Water in the abyssal basins of South Atlantic, *Russ. J. Earth Sci.*, *19,* No. 5, **Crossref**

Gamboa, L. A., R. T. Buffler, P. F. Barker (1983), Seismic Stratigraphy and Geologic History of the Rio Grande Gap and Southern Brazil Basin, *Initial Reports of the Deep Sea Drilling Project, 72 (eds. P. F. Barker, D. A. Johnson, & R. L. Carlson)* p. 481–496, U.S. Government Printing Office, Washington.

Gonthier, E., J. C. Faugères, A. Viana, et al. (2003), Upper Quaternary deposits on the Sao Tomé deep-sea channel levee system (South Brazilian Basin): Major turbidite versus contourite processes, *Marine Geology*, *199,* No. 1–2, 159–180, **Crossref**

Harloff, J., A. Mackensen (1997), Recent benthic foraminiferal associations and ecology of the Scotia Sea and Argentine Basin, *Marine Micropaleontology*, *31,* No. 1–2, 1–29, **Crossref**

Hernández-Molina, F. J., E. Llave, D. A. V. Stow (2008), Continental Slope Contourites, *Contourites. Developments in Sedimentology, 60 (eds. M. Rebesco & A. Camerlenghi)* p. 379–408, Elsevier, Amsterdam. **Crossref**

Hüneke, H., D. A. V. Stow (2008), Chapter 17 Identification of Ancient Contourites: Problems and Palaeoceanographic Significance, *Contourites. Developments in Sedimentology, 60 (eds. M. Rebesco & A. Camerlenghi)* p. 323–344, Elsevier, Amsterdam.

Ivanova, E., I. Murdmaa, D. Borisov, O. Dmitrenko, O. Levchenko, E. Emelyanov (2016), Late Pliocene – Pleistocene stratigraphy and history of formation of the Ioffe calcareous contourite drift, Western South Atlantic, *Marine Geology*, *372,* 17–30, **Crossref**

Ledbetter, M. T. (1984), Bottom-current speed in the Vema Channel recorded by particle size of sediment fine-fraction, *Marine Geology*, *58,* No. 1–2, 137–149, **Crossref**

Ledbetter, M. T. (1986), A Late Pleistocene time-series of bottom-current speed in the Vema Channel, *Palaeogeography, Palaeoclimatology, Palaeoecology*, *53,* No. 1, 97–105, **Crossref**

Levchenko, O. V., I. O. Murdmaa (2013a), Strategy of the lithological and seismoacoustic research of the deep-water deposits along transatlantic geotraverses during cruise 32 of the RV *Akademik Ioffe*, in the autumn of 2010 (Kaliningrad to Ushuaia), *Oceanology*, *53,* 124–128, **Crossref**

Levchenko, O. V., I. O. Murdmaa (2013b), Multidisciplinary investigations along the transatlantic transect Ushuaia (Argentine)–La Manche Strait: Cruise 33 of the RV *Akademik Ioffe*, *Oceanology*, *53,* No. 2, 252–257, **Crossref**

Levchenko, O. V., I. O. Murdmaa, et al. (2014), New Result of the Seismic Facies Analysis of the Quaternary Deposits in the Western Atlantic, *Doklady Earth Sciences*, *458,* No. 4, 1256–1260, **Crossref**

Lima, A. F., J. C. Faugeres, M. Mahiques (2009), The Oligocene–Neogene deep-sea Columbia Channel system in the South Brazilian Basin: Seismic stratigraphy and environmental changes, *Marine Geology*, *266,* No. 1–4, 18–41, **Crossref**

Loncke, L., L. Droz, V. Gaullier, et al. (2009), Slope instabilities from echo-character mapping along the French Guiana transform margin and Demerara abyssal plain, *Mar. Pet. Geol.*, *26,* 711–723, **Crossref**

Machado, L. C. R., R. O. Kowsmann, J. R. Almeida, et al. (1998), Abstract: Modern Turbidite System in the Campos Basin: Key to Reservoir Heterogeneities, *ABGP/AAPG International Conference and Exhibition, AAPG Bulletin* p. 82, American Association of Petroleum Geologists, Tulsa, USA.

Mackensen, A., D. K. Fütterer, et al. (1993), Benthic foraminiferal assemblages from the eastern South Atlantic Polar Front region between 35° and 57°S: Distribution, ecology and fossilization potential, *Marine Micropaleontology*, *22,* No. 1–2, 33–69, **Crossref**

Maestro, A., G. Jané, et al. (2018), Echo-character of the NW Iberian continental margin and the adjacent abyssal plains, *J. Maps*, *14,* 56–67,

Crossref

Massé, L., J.-C. Faugères, M. Bernat, A. Pujos, M.-L. Mézerais (1994), A 600,000-year record of Antarctic Bottom Water activity inferred from sediment textures and structures in a sediment core from the Southern Brazil Basin, *Paleoceanography*, *9,* No. 6, 1017–1026, Crossref

Mézerais, M. L., J.-C. Faugères, A. G. Figueiredo, L. Massé (1993), Contour current accumulation off the Vema Channel mouth, southern Brazil Basin: pattern of a "contourite fan", *Sedimentary Geology*, *82,* No. 1–4, 173–187, Crossref

Morozov, E. G., A. N. Demidov, R. Y. Tarakanov, W. Zenk (2010), *Abyssal Channels in the Atlantic Ocean, Dordrecht*, 266 pp. Springer, Netherlands. Crossref

Morozov, E. G., R. Yu. Tarakanov, et al. (2018), Currents and water strucrure north of the Vema Channel, *Russ. J. Earth Sci.*, *18,* ES5006, Crossref

Munsell Color Company (1995), *The Geological Society of America Rock Color Chart*, Rock-Color Chart Committee. Geological Society of America, Boulder, CO.

Murdmaa, I. O., D. G. Borisov, T. A. Demidova, E. V. Ivanova, O. V. Levchenko, Y. G. Marinova, A. D. Mutovkin, V. A. Putans (2012), Very High Resolution Seismic Profiling at the Brazil Margin, *Eos Transactions*, *93,* No. 25, 233–234, Crossref

Pratson, L. F., E. P. Laine (1989), The relative importance of gravity-induced versus current-controlled sedimentation during the Quaternary along the Mideast U.S. outer continental margin revealed by 3.5 kHz echo character, *Mar. Geol.*, *89,* 87–126, Crossref

Pudsey, C. J., J. A. Howe (1998), Quaternary history of the Antarctic Circumpolar Current: evidence from the Scotia Sea, *Marine Geology*, *148,* No. 1–2, 83–112, Crossref

Reid, J. L. (1989), On the total geostrophic circulation of the South Atlantic Ocean: Flow patterns, tracers, and transports, *Progress in Oceanography*, *23,* No. 3, 149–244, Crossref

Reid, J. R. (1996), On the Circulation of the South Atlantic Ocean, *The South Atlantic, G. Wefer, W. H. Berger, G. Siedler & D. J. Webb (eds.)* p. 13–44, Springer, Berlin, Heidelberg.

Reid, J. L., W. D. Nowlin, W. C. Patzert (1977), On the Characteristics and Circulation of the Southwestern Atlantic Ocean, *Journal of Physical Oceanography*, *7,* No. 1, 62–91, Crossref

Skolotnev, S. G., E. V. Ivanova, et al. (2018), Study of Seamounts and Contourite Systems of the Central and South Atlantic during Cruise 43 of the RV *Akademik Ioffe*, *Oceanology*, *58,* No. 4, 671–673, Crossref

Spooner, P. T., D. J. R. Thornalley, P. Ellis (2018), Grain Size Constraints on Glacial Circulation in the Southwest Atlantic, *Paleoceanography and Paleoclimatology*, *33,* No. 1, 21–30, Crossref

Stow, D. A. V., J.-C. Faugères (2008), Chapter 13 Contourite Facies and the Facies Model, *Contourites. Developments in Sedimentology, 60 (eds. M. Rebesco & A. Camerlenghi)* p. 223–256, Elsevier, Amsterdam. Crossref

Viana, A., A. G. Figueiredo, et al. (2003), The Sao Tomé deep-sea turbidite system (Southern Brazil Basin): Cenozoic seismic stratigraphy and sedimentary processes, *American Association of Petroleum Geologists Bulletin*, *87,* No. 5, 873–894, Crossref

Viana, A. R., J.-C. Faugères, D. A. V. Stow (1998), Bottom-current-controlled sand deposits – a review of modern shallow- to deep-water environments, *Sedimentary Geology*, *115,* No. 1–4, 53–80, Crossref

Wetzel, A., F. Werner, D. A. V. Stow (2008), Chapter 11 Bioturbation and Biogenic Sedimentary Structures in Contourites, *Contourites. Developments in Sedimentology, 60 (eds. M. Rebesco & A. Camerlenghi)* p. 183–202, Elsevier, Amsterdam. Crossref

Corresponding author:
Dmitrii G. Borisov, Shirshov Institute of Oceanology RAS, 36 Nahimovskiy pr., 117997 Moscow, Russia. (borisov.ocean@gmail.com)